

LETTER

Contactless non-destructive imaging of doping density and electrical resistivity of semiconductor Si wafers using lock-in carrierography

To cite this article: Peng Song *et al* 2018 *Semicond. Sci. Technol.* **33** 12LT01

View the [article online](#) for updates and enhancements.

Recent citations

- [Surface recombination velocity on wet-cleaned silicon wafers using heterodyne lock-in carrierography imaging: measurement uniqueness investigation](#)
Peng Song *et al*



The Electrochemical Society
Advancing solid state & electrochemical science & technology

The ECS is seeking candidates to serve as the **Founding Editor-in-Chief (EIC) of ECS Sensors Plus**, a journal in the process of being launched in 2021

The goal of ECS Sensors Plus, as a one-stop shop journal for sensors, is to advance the fundamental science and understanding of sensors and detection technologies for efficient monitoring and control of industrial processes and the environment, and improving quality of life and human health.

Nomination submission begins: May 18, 2021



Letter

Contactless non-destructive imaging of doping density and electrical resistivity of semiconductor Si wafers using lock-in carrierography

Peng Song^{1,2} , Alexander Melnikov¹, Qiming Sun^{1,3} ,
Andreas Mandelis^{1,3} and Junyan Liu²

¹ Center for Advanced Diffusion-Wave and Photoacoustic Technologies (CADIPT), University of Toronto, Toronto, M5S 3G8, Canada

² School of Mechatronics Engineering, Harbin Institute of Technology, Harbin, 150001, People's Republic of China

³ Optoelectronic Information, University of Electronic Science and Technology of China, Chengdu, 610054, People's Republic of China

E-mail: mandelis@mie.utoronto.ca

Received 28 May 2018, revised 5 October 2018

Accepted for publication 12 October 2018

Published 24 October 2018



CrossMark

Abstract

A contactless non-destructive imaging method for spatially resolved dopant concentration, [2.2] N_d , and electrical resistivity, ρ , of n - and p -type silicon wafers using lock-in carrierography images at various laser irradiation intensities is presented. Amplitude and phase information from wafer sites with known resistivity was employed to derive a calibration factor for accurate determination of the absolute carrier generation rate. A frequency-domain model based on the nonlinear nature of photocarrier radiometric signals was used to extract dopant density images. Lateral variations in the resistivity of an n -type and a p -type wafer obtained by means of this methodology were found to be in excellent agreement with those obtained with conventional 4-point probe measurements. This all-optical contactless method can be used as a non-destructive tool for doping density and electrical resistivity measurements and their images over large semiconductor areas. N_d , ρ and their variances can be measured and mapped for the photovoltaic, micro- and opto-electronic industries including on wafers with oxides or surface treated layers for which contacting electrical measurements are impossible.

Keywords: lock-in carrierography, effective lifetime, dopant concentration, resistivity

(Some figures may appear in colour only in the online journal)

Lock-in carrierography (LIC) [1], an imaging counterpart of single-element-detector photocarrier radiometry (PCR) [2], is a frequency-domain (FD) photoluminescence (PL)-based quantitative characterization technique that measures photocarrier density distributions, and has been used to characterize electronic transport properties [3–5] and electrical parameters [6, 7] in various semiconductor materials and devices. The

dopant concentration of a semiconductor is an important parameter for starting materials as well as for semiconductor devices. The conventional four-point probe method [8] and eddy current mapping [9] are commonly used to measure resistivity and/or dopant concentrations. However, the contacting nature of the four-point probe may lead to contamination and/or damage of sample surfaces. In addition, the

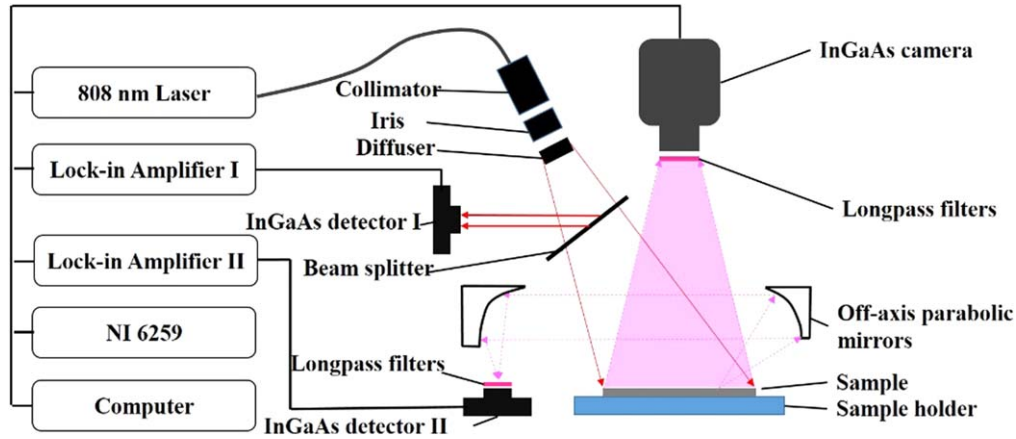


Figure 1. Schematic of the combined experimental intensity-scanned LIC and PCR system.

imaging capabilities, speed, and spatial resolution of both methods are limited due to the point-by-point mode. Recently, several luminescence-based methods have been shown to be able to measure dopant concentrations. Giesecke *et al* proposed a method to determine the dopant concentration by a dynamic PL measurement using a single-element-detector [10, 11]. Hameiri *et al* presented a method based on combined PL and photoconductance [12]. Lim *et al* proposed a method to present [13] and image [14] the total acceptor concentration of wafers by monitoring the iron-boron re-pairing rate using band-to-band PL. Mitchell *et al* introduced an imaging method to determine bulk minority carrier lifetime and doping density of silicon bricks using PL, based on a two-filter method [15]. From the ratio of two PL images using a short and a long pass filter, the bulk lifetime and then the doping density can be estimated. Very recently Sun *et al* [16] developed a FD model based on the carrier rate equation which can simultaneously determine the *effective lifetime*, τ_{eff} , *dopant concentration*, N_d , and *resistivity*, ρ , using PCR. The injection-level-dependent effective carrier lifetime was derived from PCR phase information at various intensities and then the dependence of photocarrier density versus PCR amplitude was used to fit the dopant concentration and thus calculate the *resistivity* of silicon wafers. A small-amplitude modulation depth compared to the dc level (named ‘ripple’ mode) was introduced to help bypass the complicated parameter nonlinearity problem which simplified theoretical interpretation and guaranteed measurement self-consistency and reliability. The purpose of this work is to efficiently image the dopant concentration and resistivity for silicon wafers by near-infrared camera-based LIC.

The experimental setup of the LIC system is shown in figure 1. A 9 W, 808 nm fiber-coupled diode laser was used to illuminate sample areas up to $8 \times 8 \text{ cm}^2$. The laser beam was collimated, homogenized, and spread by a microlens array across the area. Intensity scans were realized by adjusting an iris. InGaAs detector I (bandwidth: 900–1700 nm) was used to monitor the relative intensity, and an InGaAs camera (bandwidth: 900–1700 nm, 320×256 pixel, exposure time: 0.13–16.6 ms) was used to measure LIC signals. A data acquisition card (NI USB-6259) was employed to generate

reference, modulation, and camera-trigger signals. A single-element PCR system was used simultaneously with LIC system for signal consistency cross-checking purposes. An InGaAs detector (II) was used to measure PCR signals. The reflected laser beam was blocked with a 1000 nm longpass filter located in front of the camera and InGaAs detector II. The camera and the two single-element-detectors recorded signals at the same time. Two lock-in amplifiers demodulated the relative intensity and the amplitude and phase of PCR signals. Synchronous undersampling [17] with external triggering of the camera was implemented for the LIC imaging procedure. 64 frames per correlation period were scanned and used to calculate one amplitude and one phase image using in-house developed software. To validate the LIC/PCR method, the resistivity was also measured by the conventional 4-point probe method (Everbeing 4-point probe, probe spacing: 1 mm).

Two samples were measured in this work: sample I was a $290 \mu\text{m}$ thick *n*-type (phosphorus-doped) 100 mm silicon wafer with both surfaces partly passivated with amorphous-Si (α -Si). Sample II was a $690 \mu\text{m}$ thick *p*-type (boron-doped) 150 mm silicon wafer with both surfaces passivated with oxide layers. The modulation frequency was chosen to be 50 Hz for the two samples so that they would exhibit phase sensitivity to intensity and adequate camera signal-to-noise ratio (SNR). Frequency optimization was needed because the LIC/PCR phase is close to zero at low frequencies thus limiting its dynamic range, while the amplitude decreases at high frequencies, thus limiting the SNR [16, 18].

The amplitude A and phase φ of any one pixel can be expressed as [16]

$$A = \frac{C(2\Delta n_0 + N_d)\Delta n_0}{2\sqrt{1 + \omega^2\tau_{\text{eff}}^2}} \quad (1a)$$

$$\varphi = -\tan^{-1}(\omega\tau_{\text{eff}}), \quad (1b)$$

where C is a proportionality factor which takes into account the band-to-band carrier radiative recombination efficiency and the properties of the instrumentation; N_d is the dopant concentration for either *n*-type or *p*-type wafers; $\Delta n_0 = G_0\tau_{\text{eff}}$ is the dc component of the excess carrier concentration;

G_0 is the carrier generation rate; $\omega = 2\pi f$ is the angular modulation frequency; and τ_{eff} is the effective lifetime.

In this study, the depth-averaged effective lifetime τ_{eff} lumps all the carrier recombination rates together. To deal with this simplification and also the absolute carrier generation rate mentioned in [16], additionally, a calibration factor, which takes all the proportionality factors into account such as the LIC/PCR instrumentation response and the sample surface reflectivity, was employed to accurately image N_d using LIC signals from a wafer with known resistivity. Then the carrier generation rate G_0 at dc with the calibration factor can be expressed as:

$$G_0 = \frac{F_{\text{cal}} I_0 (1 - R)}{E_0 L}, \quad (2)$$

where F_{cal} is the calibration factor, I_0 is the average laser intensity, R is the wafer reflectivity (0.320 [19] for the 808 nm laser incident on the n -type Si wafer passivated with α -Si and 0.313 for the same 808 nm laser incident on the p -type Si wafer, both independently measured). E_0 is the photon energy and L is the wafer thickness.

Using equation (1b), the effective lifetime and thus Δn_0 at various G_0 can be calculated from the LIC phase. Then, the LIC amplitudes at different Δn_0 can be fitted to extract the dopant concentration N_d . For experiments, in order to derive N_d the LIC amplitude A and phase φ information at various average intensities I_0 and at fixed modulation frequency f are required, so an intensity scanned LIC measurement was performed.

In order to validate the LIC method, a comparison between PCR and LIC from a specific location on the n -type wafer labeled ‘Point A’ is shown in figure 2. Figures 2(a) and (b) show the dependence of amplitude and phase on intensity, respectively. From figure 2(b) it is observed that for this wafer, camera pixel phases and the single-element-detector are sensitive to intensity at 50 Hz. Therefore, the lifetime dependence on excess minority carrier concentration could be calculated through equation (1b). The small phase difference between LIC and PCR may be caused by (1) the difference in the size of the detected area: for LIC imaging the detected area was 0.2 mm for each pixel determined by the camera pixel resolution, objective, and focal distance, while for PCR the detected area was 1 mm diameter determined by the area of the single-element-detector and the size of the off-axis paraboloidal mirrors; (2) the different software used for the digital LIC signal demodulation and for the hardware lock-in PCR demodulation. The effects of these small phase differences on lifetime calculation and on the derivation of N_d will be discussed below. The inset images in figures 2(a) and (b) are amplitude and phase, respectively, at 649 W m^{-2} laser intensity. An inhomogeneous excess carrier concentration distribution can be clearly distinguished. Figure 2(c) shows the effective lifetime dependence on intensity as directly calculated from equation (1b). The inset image in figure 2(c) is that of the effective lifetime, also at 649 W m^{-2} . This inset directly corresponds to the phase image in figure 2(b). In order to precisely measure N_d and ρ with this method, Point A

with known resistivity measured as per the established electrical procedure outlined in [20], was chosen to derive the appropriate instrumental calibration factor F_{cal} for the LIC measurement. The latter was found to be $F_{\text{cal}} = 0.65$ for consistency with the 4-point probe result at Point A acting as a reference measurement. This calibration factor was also applied to the PCR measurements and also for the p -type wafer. The dependence of the normalized amplitude on the calibrated Δn_0 is shown in figure 2(d), where ‘normalized amplitude’ means the measured amplitude multiplied with the coefficient $\sqrt{1 + \omega^2 \tau_{\text{eff}}^2}$, by virtue of equation (1a). This dependence was then fitted to equation (1a) in order to extract N_d . From figure 2(d), the N_d and ρ values measured with PCR were found to be exactly consistent with those measured with LIC and also in good agreement with the 4-point probe measurements as shown in table 1. Therefore, the effect of the aforementioned small phase differences between LIC and PCR at fixed intensity on the N_d and ρ could be neglected. Following the calculation of the dopant concentration for all pixels, the quantitative dopant concentration image was constructed and is shown as an inset in figure 2(d). The distribution of dopant concentration was found to have a correlation with the effective carrier lifetime image inset in figure 2(c), in agreement with the expectation that the latter represents the bulk carrier lifetime because the distribution of surface recombination velocities can be assumed homogeneous and low due to the amorphous silicon surface passivation process. This correlation shows that doping variations have a direct effect on semiconductor substrate electronic properties and make doping imaging metrologies like LIC essential for monitoring and controlling the doping process.

Figure 3 shows the results for the p -type wafer with both surfaces passivated with thick oxide layers. ‘Point B’ was selected for comparison between PCR and LIC. The dependencies of amplitude, phase and lifetime on intensity are shown in figures 3(a)–(c), respectively. The dependence of normalized amplitude on calibrated Δn_0 is shown in figure 3(d). Similar to the n -type sample I, the dopant concentration N_d obtained by means of PCR is in good agreement with its LIC counterpart. The inset images in figure 3 represent amplitude, phase, and lifetime at 638 W m^{-2} , and the best-fitted N_d .

From the N_d images in figures 2(d) and 3(d), the resistivity images of both samples were derived and are shown in figures 4(a) and (b). They were obtained using the following equations:

For boron-doped Si, the doping density is related to the resistivity by [20]

$$\rho = \frac{1.305 \times 10^{16}}{N_d} + \frac{1.133 \times 10^{17}}{N_d [1 + (2.58 \times 10^{-19} N_d)^{-0.737}]} (\Omega \text{ cm}). \quad (3)$$

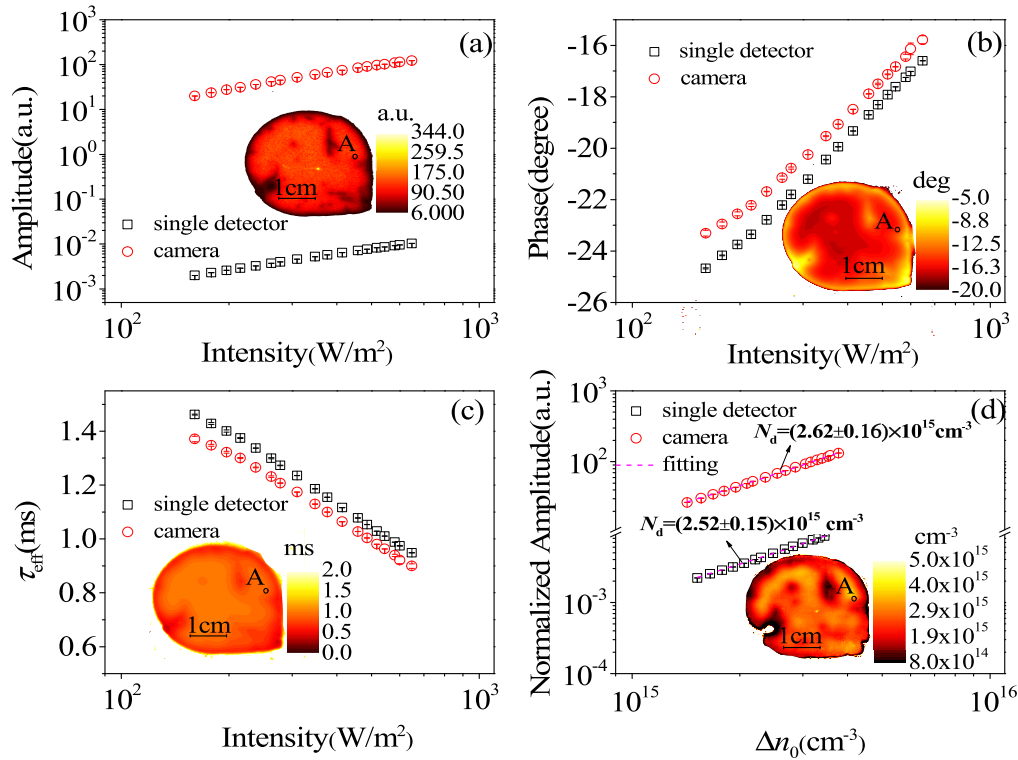


Figure 2. PCR and LIC comparison at a selected position (Point A) on a *n*-type Si wafer with both sides passivated: laser intensity dependence of amplitude (a), phase (b), and effective lifetime (c). Dependence of normalized amplitude (d) on photocarrier concentration and the corresponding best-fitted curves. Normalized amplitude is the measured amplitude multiplied by $\sqrt{1 + \omega^2 \tau_{\text{eff}}^2}$, equation (1a). Modulation frequency: 50 Hz. The inset images are amplitude (a), phase (b), lifetime (c) at 649 W m^{-2} , and the best-fitted N_d (d).

Table 1. Comparison of resistivity values measured by the three techniques.

Measurement technique	4-point probe	LIC	PCR
Point A ($\Omega \text{ cm}$)	1.65 ± 0.07	1.65 ± 0.10	1.71 ± 0.09
Point B ($\Omega \text{ cm}$)	35.14 ± 1.45	33.65 ± 2.02	31.99 ± 1.92

For phosphorus-doped Si, the doping density is related to the resistivity by [20]

$$\rho = \frac{6.242 \times 10^{18} 10^Z}{N_d} (\Omega \text{ cm});$$

$$Z = \frac{C_0 + C_1 y + C_2 y^2 + C_3 y^3}{1 + D_1 y + D_2 y^2 + D_3 y^3}, \quad (4)$$

where [2.1] $y = \log_{10}(N_d) - 16$, $C_0 = -3.0769$, $C_1 = 2.2108$, $C_2 = -0.62272$, $C_3 = -0.057501$, $D_1 = -0.68157$, $D_2 = 0.19833$, $D_3 = -0.018376$.

In order to validate our quantitative resistivity image, after removing the oxide layers the 4-point probe method was used to measure the resistivity at several points on both samples and the results were compared to the LIC profiles. The comparison involved contiguous LIC and discrete 4-point probe measurements along the vertical lines at 0 cm shown in figures 4(a) and (b). In figure 5 the shown continuous line and width of the LIC resistivity profile represent the mean value and the variance across a 5 mm wide strip of

pixels. It is observed that the LIC results are in excellent agreement with the 4-point probe (R^2 value = 0.9755 for the *n*-type wafer and 0.9979 for the *p*-type wafer). Additionally, the LIC resistivity exhibits better spatial resolution than the 4-point probe that depends only on pixel size. This feature can be an advantage for accurate monitoring of the doping distribution of semiconductors in a non-contact manner throughout the doping process. However, the excess carrier concentration detection SNR in LIC imaging limits its ability to measure dopant concentrations. Specifically, the method requires that the range of the injected excess carrier concentration should be on the order of the doping density, N_d . In turn, the excess carrier concentration is determined by the effective lifetime and generation rate. From our previous studies, lifetimes as low as several hundreds of ns can be measured using LIC/PCR [5, 21]. For heavily doped samples, precise determination of dopant concentrations also requires measurement of the associated excess carrier concentration. However, the determination of dopant concentrations in almost intrinsic wafers with high resistivity can be challenging due to the low injected excess carrier densities and the concomitant low SNR.

In summary, an all optical contactless non-destructive LIC method for imaging semiconductor dopant concentration and resistivity was presented. Good agreement between the LIC images and the conventional electrical 4-point-probe method was found for *n*- and *p*-type Si wafers. This quantitative imaging modality may become a candidate for

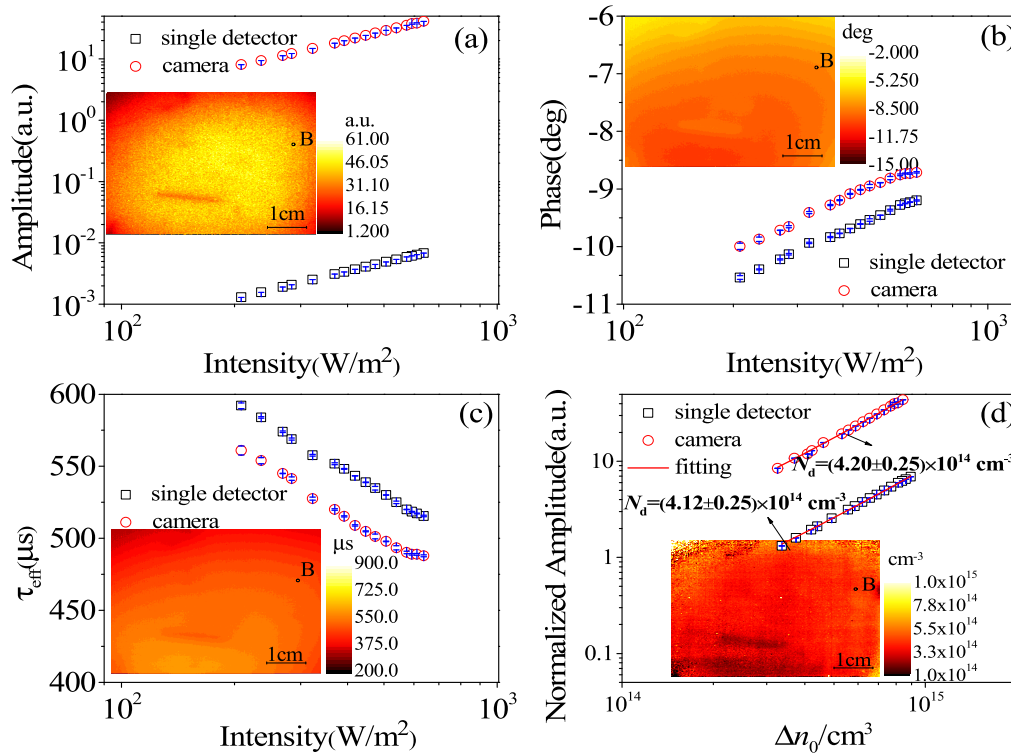


Figure 3. PCR and LIC comparison at a selected position (Point B) on a *p*-type Si wafer: laser intensity dependence of amplitude (a), phase (b), and effective lifetime (c). Dependence of normalized amplitude (d) as in figure 2 on photocarrier concentration and the corresponding best-fitted curves. Modulation frequency: 50 Hz. The inset images are amplitude (a), phase (b), lifetime (c) at 638 W m^{-2} , and the best-fitted N_d (d).

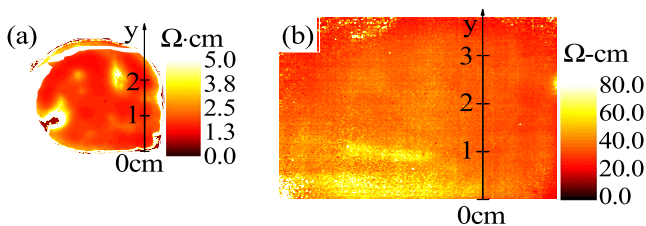


Figure 4. Resistivity images of the *n*-type wafer (a) and *p*-type wafer (b).

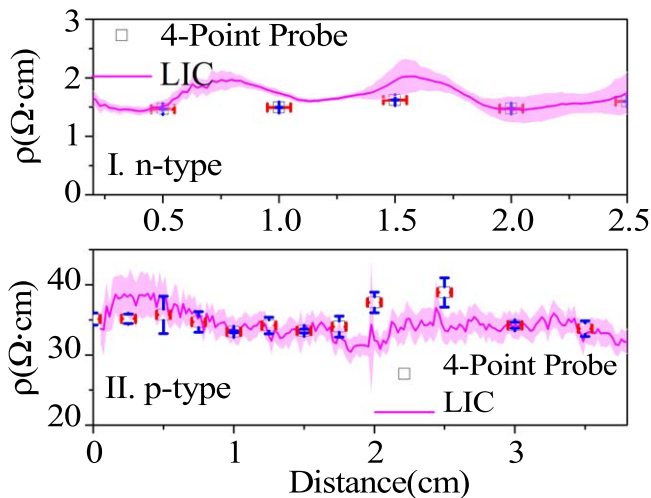


Figure 5. Resistivity profile comparison between LIC and 4-point probe along the vertical lines at 0 cm in figure 4.

providing spatially resolved information on dopant concentration and resistivity of semiconductor substrates in industrial wafer fab settings. It paves the way for applications in the photovoltaic, micro- and opto-electronic industries and also provides a highly efficient way to measure N_d , ρ and their variances on wafers with oxide or surface treated layers for which contacting electrical measurements are impossible. For on-line inspection, the measurement time can be greatly reduced (< 1 min) by automatic laser intensity changes and decrease in the number of captured frames per correlation period.

Acknowledgments

A Mandelis is grateful to the Natural Sciences and Engineering Research Council of Canada (NSERC) for a Discovery grant, to the Canada Research Chairs Program, and to the Chinese Recruitment Program of Global Experts (Thousand Talents). PS and JYL acknowledge the National Natural Science Foundation of China (Grant no. 61571153). PS also acknowledge the financial support from China Scholarship Council.

ORCID iDs

Peng Song  <https://orcid.org/0000-0002-6029-945X>

Qiming Sun  <https://orcid.org/0000-0003-1184-3719>

References

- [1] Melnikov A, Mandelis A, Tolev J, Chen P and Huq S 2010 *J. Appl. Phys.* **107** 114513
- [2] Mandelis A, Batista J and Shaughnessy D 2003 *Phys. Rev. B* **67** 205208
- [3] Sun Q M, Melnikov A and Mandelis A 2012 *Appl. Phys. Lett.* **101** 242107
- [4] Sun Q M, Melnikov A, Mandelis A and Pagliaro R H 2018 *Appl. Phys. Lett.* **112** 012105
- [5] Hu L L, Liu M X, Mandelis A, Sun Q M, Melnikov A and Sargent E H 2018 *Sol. Energy Mater. Sol. Cells* **174** 405
- [6] Liu J Y, Melnikov A and Mandelis A 2013 *J. Appl. Phys.* **114** 104509
- [7] Song P, Liu J Y, Mohummad O and Wang Y 2017 *Phys. Status Solidi* **11** 1700153
- [8] Valdes L B 1954 *Proc. IRE* **42** 420
- [9] Schroder D K 1998 *Semiconductor Material and Device Characterization* (New York: Wiley) p 36
- [10] Giesecke J A, Walter D, Kopp F, Rosenits P, Schubert M C and Warta W 2010 Simultaneous determination of carrier lifetime and net dopant concentration of silicon wafers from photoluminescence *Proc. 35th IEEE Photovoltaic Specialists Conf. (Honolulu)* pp 847–51
- [11] Giesecke J A, Schubert M C and Warta W 2012 *J. Appl. Phys.* **112** 063704
- [12] Hameiri Z, Trupke T, Gao N, Sinton R A and Weber J W 2013 *Prog. Photovolt., Res. Appl.* **21** 942–9
- [13] Lim S Y and Macdonald D 2011 *Sol. Energy Mater. Sol. Cells* **95** 2485
- [14] Lim S Y, Phang S P, Trupke T, Cuevas A and Macdonald D 2011 *J. Appl. Phys.* **110** 113712
- [15] Mitchell B, Trupke T, Weber J W and Nyhus J 2011 *J. Appl. Phys.* **109** 083111
- [16] Sun Q M, Melnikov A, Wang J and Mandelis A 2018 *J. Phys. D: Appl. Phys.* **51** 15LT01
- [17] Breitenstein O, Warta W and Langenkamp M 2010 *Lock-In Thermography* (Berlin: Springer) p 18
- [18] Mandelis A 2001 *Diffusion-Wave Fields: Mathematical Methods and Green Functions* (New York: Springer) pp 584–97 ch 9
- [19] Green M A and Keevers M J 1995 *Prog. Photovolt., Res. Appl.* **3** 189–92
- [20] Schroder D K 2006 *Semiconductor Material and Device Characterization* (New York: Wiley) pp 41–3
- [21] Wang J, Mandelis A, Sun Q, Li B and Gao C 2018 *J. Phys. Chem. C* **122** 5759